COMPDYN 2011
3^{rd} ECCOMAS Thematic Conference on
Computational Methods in Structural Dynamics and Earthquake Engineering
M. Papadrakakis, M. Fragiadakis, V. Plevris (eds.)
Corfu, Greece, 25-28 May 2011

DYNAMIC RUPTURE MODELLING ON UNSTRUCTURED MESHES USING A DISCONTINUOUS GALERKIN METHOD

Christian Pelties[1] **and Martin Käser**[1,2]

[1]Geophysics - Department of Earth and Environmental Sciences
Ludwig-Maximilians-Universität München
Theresienstrasse 41
80333 München - Germany
e-mail: pelties@geophysik.uni-muenchen.de

[2]Geo Risk - Münchener Rückversicherungs-Gesellschaft
Königinstrasse 107
80802 München - Germany
e-mail: mkaeser@munichre.com

Keywords: Dynamic Rupture, Source Physics, Earthquake Dynamics, Seismic Wave Propagation, Computational Seismology.

Abstract. *We will present recent developments concerning the extensions of the ADER-DG method to solve three dimensional dynamic rupture problems on unstructured tetrahedral meshes. A remarkable feature of this method is the combination of the DG scheme and a time integration method using Arbitrarily high-order DERivatives (ADER) to provide high accuracy in space and time with the discretization on unstructured meshes. In the resulting discrete velocity-stress formulation of the elastic wave equations variables are naturally discontinuous at the interfaces between elements. The so-called Riemann problem can then be solved to obtain well-defined values of the variables at the discontinuity itself. This is in particular valid for the fault at which a given friction law has to be evaluated. Hence, the fault's geometry is honored by the computational mesh. This way, complex fault planes can be modeled adequately with small elements while fast mesh coarsening is possible with increasing distance from the fault. A further advantage of the scheme is that it avoids spurious high-frequency contributions in the slip rate spectra and therefore does not require artificial Kelvin-Voigt damping or filtering of synthetic seismograms.*

1 INTRODUCTION

Strong ground motion models for seismic hazard assessment are based on the understanding of earthquake sources and seismic wave propagation. The state of the art is the combination of earthquake dynamics together with wave propagation in a single simulation. Synergy effects are for instance basin effects on wave propagation from finite-extent earthquake sources, high-frequency source directivity in random media and in highly heterogeneous fault zones, and rupture propagation of and seismic radiation from dynamic source models on non-planar faults utilizing slip-weakening and rate-and-state friction models.

A variety of numerical methods have been used in the past to implement the dynamics of earthquake rupture, such as finite differences (FD) [1, 2, 3], boundary integral (BI) [4, 5], finite volume (FV) [6], or spectral element (SE) [7], to name only a few commonly used methodologies. All these techniques have certain advantages and drawbacks. The most accurate and efficient method is the BI method, but it is in general not suited for handling heterogeneous media and nonlinear materials. FD schemes provide flexibility in terms of the choice in the friction law or in different material properties. However, it is difficult to apply them to non-planar faults, and computational resource issues could occur when strong material contrasts are included in the model, like sedimentary basins with extremely low wave velocities. FV methods are geometrically flexible but are only implemented as low-order accurate operators that are very dispersive. This fact affects the wave form in the nearfield and in turn the rupture front evolution. The SE method is both accurate and flexible and well suited for seismic wave propagation, but is restricted to hexahedral element types. The generation of hexahedral meshes for complicated geometries in three dimensions, such as faults with branching, and adapting smoothly the element sizes to different material properties, are still very challenging tasks and a major bottleneck.

J. de la Puente [8] presented recently an alternative for the dynamic rupture problem, based upon a discontinuous Galerkin (DG) method combined with an arbitrary high-order derivatives (ADER) time integration [9]. The DG method combines features from high-order FV and finite element methods, where a polynomial basis is used inside each element to approximate the physical variables of the elastic wave equations. This formulation enables the use of fully unstructured meshes, i.e. triangles (2D) or tetrahedrons (3D), to better fit the constraints of a given model and in particular the fault shape. Another feature of DG methods, inherited from FV methods, is the concept of numerical fluxes at element interfaces. Between any two elements the variables of the elastic wave equations are discontinuous. This is valid, as the exact solution of the elastic wave equations at a discontinuity exists, and is obtained by the solution of the well-known Riemann problem [10, 11]. At a fault the solution of the Riemann problem has to be modified to take the frictional boundary conditions into consideration. The numerical dispersion properties of a DG method and the high accuracy of the flux concept for high-order formulations are the reasons why the solution of the ADER-DG method is relatively smooth and free of spurious high-frequency oscillations compared to other methods. Therefore, it does not require artificial Kelvin-Voigt damping or filtering of the seismograms. This is an important feature, since the damping reduces the time step of a simulation and, thus, increases the computational runtime significantly.

The extension of the scheme to three dimensional problems on tetrahedral meshes was presented by *C. Pelties* [12]. In this paper, we present recent developments.

2 DYNAMICS OF FAULT RUPTURE

The kinematics of a sliding process can be described by the slip rate $\Delta v = v^+ - v^-$, where $v^{+,-}$ are the velocities parallel to the fault, and the slip Δd, so that $\Delta v = \Delta \dot{d}$. We denote τ and σ the absolute shear and normal stresses on the fault, respectively.

Slip starts when the shear stress on the fault overcomes the fault strength. In the Coulomb friction model adopted here the strength is proportional to the normal stress. During active slip, the slip rate and the shear traction have opposite directions. These three phenomena are accounted for in the following expressions:

$$\begin{aligned} |\tau| &\leq \mu_f \sigma \,, \\ (|\tau| - \mu_f \sigma)\, \Delta v &= 0 \,, \\ \Delta v |\tau| + |\Delta v| \tau &= 0 \,, \end{aligned} \tag{1}$$

where μ_f is the friction coefficient. We adopt the linear slip weakening friction law [13]:

$$\mu_f = \begin{cases} \mu_s - \dfrac{\mu_s - \mu_d}{D_c} \Delta d & \text{if } \Delta d < D_c \,, \\ \mu_d & \text{if } \Delta d \geq D_c \,. \end{cases} \tag{2}$$

With increasing slip Δd the friction coefficient μ_f drops from the static value μ_s to the dynamic μ_d over the critical slip distance D_c, as shown in Fig. 1. Although we chose a simple friction law for demonstration reasons, the ADER-DG method is able to support any friction law.

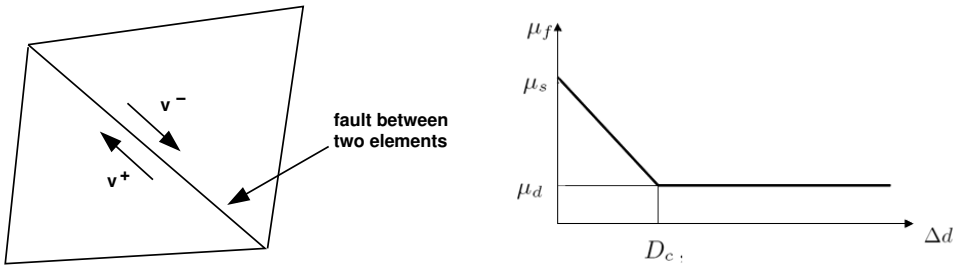

Figure 1: The left sketch gives an idea about how a fault increment is respected by the mesh. The different sides are indicated by plus and minus. On the right we plot μ_f vs. Δd for the linear slip weakening friction law.

3 FAULT DYNAMICS WITHIN THE DISCONTINUOUS GALERKIN FRAMEWORK

In contrast to other dynamic rupture implementations, like traction-at-split-node which is popular for FD methods, *J. de la Puente* [8] followed a new approach employing the concept of fluxes. In this section, we will explain the basic ideas behind this and show the extension to three-dimensional problems.

3.1 Elastic wave equations in velocity-stress formulation

Omitting external sources (e.g. moments or body forces), the three-dimensional elasticity for an isotropic medium are written in velocity-stress form as the linear hyperbolic system

$$\begin{aligned}
\tfrac{\partial}{\partial t}\sigma_{xx} - (\lambda+2\mu)\tfrac{\partial}{\partial x}u - \lambda\tfrac{\partial}{\partial y}v - \lambda\tfrac{\partial}{\partial z}w &= 0\,,\\
\tfrac{\partial}{\partial t}\sigma_{yy} - \lambda\tfrac{\partial}{\partial x}u - (\lambda+2\mu)\tfrac{\partial}{\partial y}v - \lambda\tfrac{\partial}{\partial z}w &= 0\,,\\
\tfrac{\partial}{\partial t}\sigma_{zz} - \lambda\tfrac{\partial}{\partial x}u - \lambda\tfrac{\partial}{\partial y}v - (\lambda+2\mu)\tfrac{\partial}{\partial z}w &= 0\,,\\
\tfrac{\partial}{\partial t}\sigma_{xy} - \mu(\tfrac{\partial}{\partial x}v + \tfrac{\partial}{\partial y}u) &= 0\,,\\
\tfrac{\partial}{\partial t}\sigma_{yz} - \mu(\tfrac{\partial}{\partial z}v + \tfrac{\partial}{\partial y}w) &= 0\,,\\
\tfrac{\partial}{\partial t}\sigma_{xz} - \mu(\tfrac{\partial}{\partial z}u + \tfrac{\partial}{\partial x}w) &= 0\,,\\
\rho\tfrac{\partial}{\partial t}u - \tfrac{\partial}{\partial x}\sigma_{xx} - \tfrac{\partial}{\partial y}\sigma_{xy} - \tfrac{\partial}{\partial z}\sigma_{xz} &= 0\,,\\
\rho\tfrac{\partial}{\partial t}v - \tfrac{\partial}{\partial x}\sigma_{xy} - \tfrac{\partial}{\partial y}\sigma_{yy} - \tfrac{\partial}{\partial z}\sigma_{yz} &= 0\,,\\
\rho\tfrac{\partial}{\partial t}w - \tfrac{\partial}{\partial x}\sigma_{xz} - \tfrac{\partial}{\partial y}\sigma_{yz} - \tfrac{\partial}{\partial z}\sigma_{zz} &= 0\,,
\end{aligned} \tag{3}$$

where λ is the first Lamé constant and μ is the shear modulus. ρ indicates the density. The normal stress components are given by σ_{xx}, σ_{yy}, and σ_{zz}, and the shear stresses are σ_{xy}, σ_{yz}, and σ_{xz}. The components of the particle velocities in the x-, y-, and z-directions are denoted by u, v and w, respectively. These nine equations are sufficient to describe the complete wave field developing with time as described in detail in *Dumbser et al.* [14].

The physical variables $Q = (\sigma_{xx}, \sigma_{yy}, \sigma_{zz}, \sigma_{xy}, \sigma_{yz}, \sigma_{xz}, u, v, w)^T$ are approximated in the DG approach within a tetrahedral element $T^{(m)}$ by high-order polynomials

$$Q_p^m(x,y,z,t) = \hat{Q}_{pl}^m(t)\Phi_l(x,y,z)\,, \tag{4}$$

where Φ_l are orthogonal basis functions. Therefore, the physical variables are expressed within the DG scheme by a linear combination of these basis functions and time-dependent degrees of freedom $\hat{Q}_{pl}^m(t)$. The index p is associated with the unknowns in the vector Q and l indicates the l-th basis function.

3.2 Riemann problem

As mentioned above, between any two elements the variables of the elastic wave equations are in general discontinuous. This kind of problem, a discontinuous initial condition together with a partial differential equation, is called the Riemann problem. The solution of the Riemann problem at an element interface is the Godunov state and can be written in terms of explicit

values as [8, 10, 11]

$$\begin{aligned}
\sigma^G_{xx} &= (\sigma^+_{xx} + \sigma^-_{xx})/2 + \tfrac{c_p\rho}{2}(u^- - u^+)\,, \\
\sigma^G_{yy} &= \sigma^+_{yy} + (\sigma^G_{xx} - \sigma^+_{xx})(1 - \tfrac{2c_s^2}{c_p^2})\,, \\
\sigma^G_{zz} &= \sigma^+_{zz} + (\sigma^G_{xx} - \sigma^+_{xx})(1 - \tfrac{2c_s^2}{c_p^2})\,, \\
\sigma^G_{xy} &= (\sigma^+_{xy} + \sigma^-_{xy})/2 + \tfrac{\mu}{2c_s}(v^- - v^+)\,, \\
\sigma^G_{yz} &= \sigma^+_{yz}\,, \\
\sigma^G_{xz} &= (\sigma^+_{xz} + \sigma^-_{xz})/2 + \tfrac{\mu}{2c_s}(w^- - w^+)\,, \\
u^G &= u^+ + \tfrac{1}{c_p\rho}(\sigma^G_{xx} - \sigma^+_{xx})\,, \\
v^G &= (v^+ + v^-)/2 + \tfrac{c_s}{2\mu}(\sigma^-_{xy} - \sigma^+_{xy})\,, \\
w^G &= (w^+ + w^-)/2 + \tfrac{c_s}{2\mu}(\sigma^-_{xz} - \sigma^+_{xz})\,.
\end{aligned} \tag{5}$$

We assume that the fault is located exactly in the XZ-plane and ruptures purely in the Y-direction. Hence, we have to impose the shear stress σ_{xy} according to the friction law Eq. 2 and obtain the new traction value $\tilde{\sigma}_{xy}$, which in the case of rupture is different from σ^G_{xy}. In turn, this provides boundary conditions for the fault parallel-velocities. Multiplying the fourth equation of Eq. 5 by c_S/μ and subtracting the eighth equation leads to

$$\tilde{v}^+ = v^+ + \frac{c_s}{\mu}\left(\tilde{\sigma}_{xy} - \sigma^+_{xy}\right) \quad \text{and} \quad \tilde{v}^- = v^- - \frac{c_s}{\mu}\left(\tilde{\sigma}_{xy} - \sigma^-_{xy}\right)\,, \tag{6}$$

when we substitute σ^G_{xy} with its imposed value $\tilde{\sigma}_{xy}$. $\tilde{v}^-$ is obtained by summing the equations instead of subtracting them.

These expressions are crucial for the understanding of fault dynamics using fluxes, as they state that an imposed traction instantly and locally generates an imposed velocity parallel to the fault. By subtracting them, the slip rate is obtained:

$$\Delta\tilde{v} = \frac{2c_s}{\mu}\left(\tilde{\sigma}_{xy} - \sigma^G_{xy}\right)\,. \tag{7}$$

This way, the analytical form of the fault tractions is captured.

4 VERIFICATION

For most of the dynamic rupture problems there does not exist an analytical reference solution for comparison. Therefore, the Southern California Earthquake Center (SCEC) created the Dynamic Earthquake Rupture Code Verification Exercise, where different codes and methodologies are compared [15]. Here, we verify our method with the Test Problem Version 3 (TPV3).

4.1 The SCEC test case

The TPV3 uses the slip-weakening friction law in Eq. 2 and rupture on a stress-homogeneous vertical strike-slip fault set in a homogeneous full-space. The initial shear and normal stresses

are assigned to be homogeneous for the 30 km long by 15 km deep fault as shown in Fig. 2, with the exception of the nucleation zone that has higher initial shear stresses. The parameters can be found in Table 1. Rupture is not allowed beyond the fault boundaries. This fault is embedded in a large computational domain of 72 km width in each spatial dimension to avoid spurious reflections from non-perfectly absorbing boundaries.

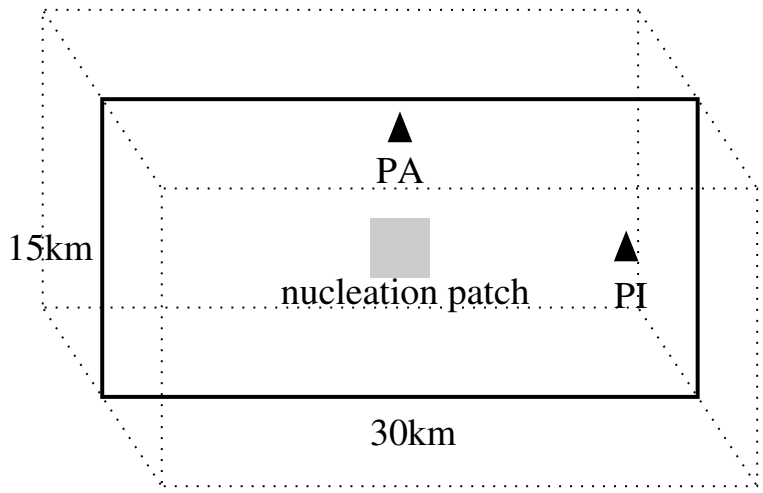

Figure 2: Sketch of the SCEC test case with the nucleation zone (grey shaded). The fault is surrounded by a box with an edge length of 72 km. The black triangles indicate the in-plane receiver (PI) and the anti-plane receiver (PA).

Parameter	Nucleation Zone	Outside Nucleation Zone
Initial shear traction (MPa)	81.6	70.0
Initial normal stress (MPa)	120.0	120.0
Static friction coefficient	0.677	0.677
Dynamic friction coefficient	0.525	0.525
Critical slip distance (m)	0.4	0.4

Table 1: Parameters describing the fault for the SCEC test case.

4.2 Results

In Fig. 3 we compare our solution (red line) with the solution of *Day et al.* [2] (black line) which was well validated during the SCEC exercises. *Day et al.* used a FD staggered-grid split node method of accuracy order 2 with a 50 m grid interval (DFM0.05). The solution produced with our DG scheme is of accuracy order 3 (ADER-DGO3) and uses a triangular mesh with an edge length of 300 m to discretize the fault, but we allow for tetrahedrons with 600 m edge length around the fault in a small box of 10 km thickness. This box is embedded in the domain of 72 km side length where we let the element edge length of the tetrahedrons quickly increase from 600 m to 3000 m to reduce the computational effort. No artificial reflexions possibly caused by the mesh coarsening are observed.

The ADER-DG solution is in excellent agreement with the solution produced by DFM0.05. This includes the arrival time of the stopping face and the stress relaxation. Furthermore, in

Fig. 4 we see that the spectral behavior of the ADER-DG slip rate solution shows the theoretically expected frequency decay [16]. No spurious high-frequency oscillations are produced. Therefore, no artificial Kelvin-Voigt damping has to be applied which would further reduce the time step size and increase the computational effort.

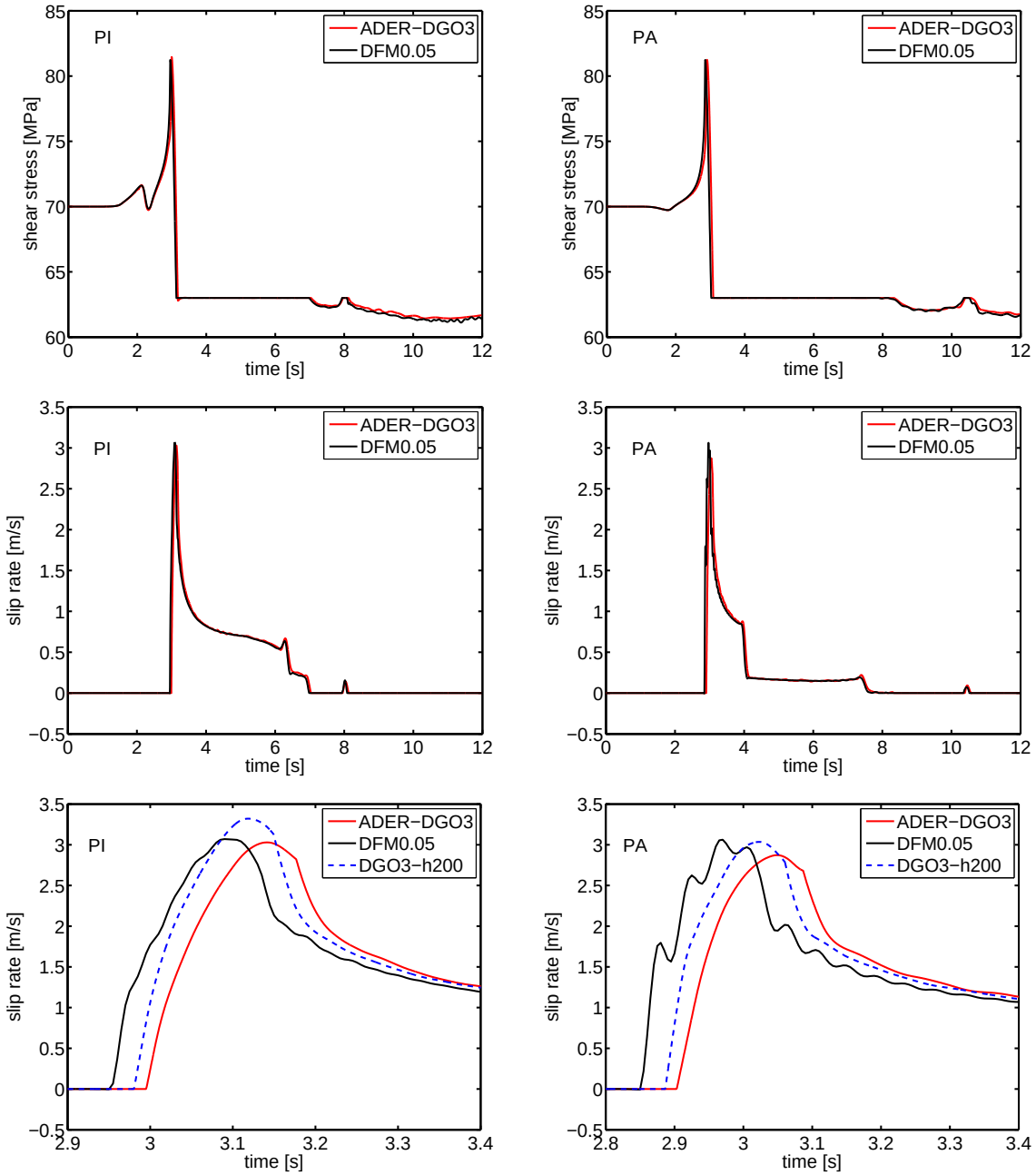

Figure 3: DFM0.05 (black line) indicates the FD staggered-grid split node method with 50 m grid interval of *Day et al.* [2]. This solution is in well agreement with the solution produced by our ADER-DGO3 scheme (red line) and a mesh spacing of 300 m at the fault. Shown is the shear stress and the slip rate. PI and PA denote the in-plane and the anti-plane receiver as shown in Fig. 2. In the bottom row we additionally plot the solution obtained with a 200 m fault discretization DGO3-h200 (blue dashed line) also with order 3 to demonstrate the trend of a convergence towards the DFM0.05 solution with increasing mesh refinement.

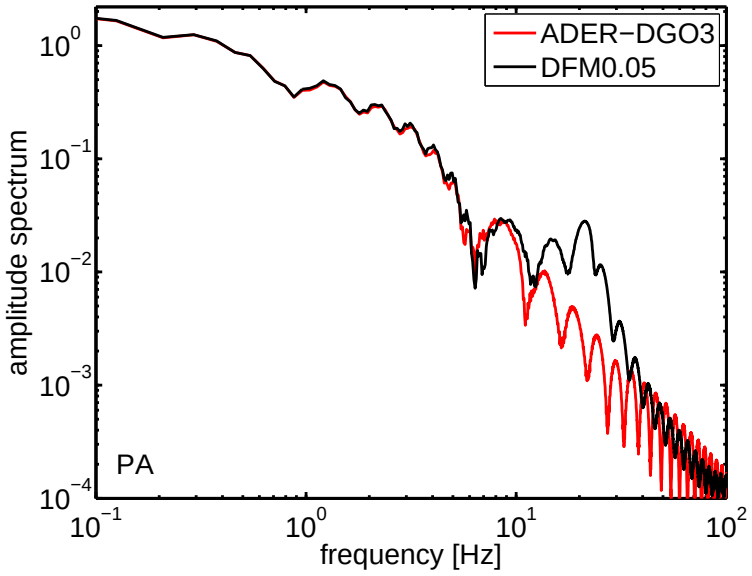

Figure 4: Spectrum of the slip rate obtained from receiver PA. The ADER-DGO3 solution does not show spurious high-frequency oscillations and, furthermore, it follows the frequency decay as theoretically expected.

5 CONCLUSIONS

We showed the successful adaption of 3D fault dynamics in the ADER-DG scheme under linear slip weakening friction. Accuracy was verified by employing the SCEC benchmark TPV3 for spontaneous rupture. Due to the properties of the Riemann problem in terms of the smoothness of the solution, the slip rate spectra remains free of spurious high-frequency oscillations. Furthermore, our implementation of the fault dynamics employing fluxes should allow for fault branching and surface rupture with little additional effort.

We conclude that the combination of meshing flexibility and high-order accuracy of the ADER-DG method will make it a very useful tool to study earthquake dynamics on complex fault systems. Future steps in the development could be the incorporation of bimaterial fault interfaces and more complex friction laws like rate- and state-dependent friction.

6 ACKNOWLEDGMENT

The authors thank the DFG (Deutsche Forschungsgemeinschaft), as the work was supported through the *Emmy Noether-Programm* (KA 2281/2-1). The data used for comparison in section 4.2 was provided by Luis A. Dalguer. Furthermore, we thank Luis A. Dalguer, Jean-Paul Ampuero, Cristóbal E. Castro and Josep de la Puente for very helpful and fruitful discussions. We also thank M. Mai for providing computational resources as many parallel tests and the SCEC benchmark have been computed on the BlueGene/P *Shaheen* of the King Abdullah University of Science and Technology, Saudi Arabia.

REFERENCES

[1] D.J. Andrews, A numerical study of tectonic stress release by underground explosions, *Bull. Seism. Soc. Am.*, 63, 1375-1391, 1973.

[2] S.M. Day, L.A. Dalguer, N. Lapusta and Y. Liu, Comparison of finite difference and boundary integral solutions to three-dimensional spontaneous rupture, *J. Geophys. Res*, 110, 2005, B12307.

[3] P. Moczo, J. Kristek, M. Galis, P. Pazak and M. Balazovjech, The Finite-difference and Finite-element modeling of seismic wave propagation and earthquake motion, *Acta physica slovaca*, 57(2), 177-406, 2007.

[4] S. Das, A numerical method for determination of source time functions for general three-dimensional rupture propagation, *Geophys. J. Roy. Astr. Soc.*, 62, 591-604, 1980.

[5] N. Lapusta, J.R. Rice, Y. Ben-Zion and G. Zheng, Elastodynamic analysis for slow tectonic loading with spontaneous rupture episodes on faults with rate- and state-dependent friction, *J. Geophys. Res*, 105, 23765-23789, 2000.

[6] M. Benjemaa, N. Glinsky-Olivier, V.M. Cruz-Atienza, J. Virieux and S. Piperno, Dynamic non-planar crack rupture by a finite volume method, *Geophys. J. Int.*, 171, 271-285, 2007.

[7] J.-P. Ampuero, Etude physique et numérique de la nucléation des séismes, Ph.D. thesis, Université Paris 7, Denis Diderot, 2002.

[8] J. de la Puente, J.-P. Ampuero and M. Käser, Dynamic rupture modeling on unstructured meshes using a discontinuous Galerkin method, *J. Geophys. Res*, 114, B10302, 2009.

[9] V.A. Titarev and E.F. Toro, ADER: Arbitrary high order Godunov approach, *J. Sci. Comput.*, 17, 609-618, 2002.

[10] E.F. Toro, *Riemann Solvers and Numerical Methods for Fluid Dynamics*, Springer, Berlin, 1999.

[11] R.L. LeVeque, *Finite Volume Methods for Hyperbolic Problems*, Cambridge University Press, Cambridge, U.K., 2002.

[12] Pelties, C., J. de la Puente and M. Käser, *Dynamic Rupture Modeling in Three Dimensions on Unstructured Meshes Using a Discontinuous Galerkin Method*, Abstract S21C-2068, AGU 2010 Fall Meeting, San Francisco.

[13] Y. Ida, Cohesive force across the tip of a longitudinal-shear crack and Griffith's specific surface energy, *J. Geophys. Res*, 77, 3796-3805, 1972.

[14] M. Dumbser and M. Käser, An Arbitrary High Order Discontinuous Galerkin Method for Elastic Waves on Unstructured Meshes II: The Three-Dimensional Case, *Geophys. J. Int.*, 167(1), 319-336, 2006.

[15] R.A. Harris, R. Archuleta, B. Aagaard, J.-P. Ampuero, D.J. Andrews, L. Dalguer, S. Day, E. Dunham, G. Ely, Y. Kase, N. Lapusta, Y. Liu, S. Ma, D. Oglesby, K. Olsen and A. Pitarka, *The source physics of large earthquakes: Validating spontaneous rupture methods*, Eos Trans. AGU, 85, 47, Fall Meet. Suppl., Abstract S12A-05, 2004.

[16] Y. Ida, The maximum acceleration of seismic ground motion, *Bull. Seism. Soc. Am.*, 63, 959-968, 1973.